Anaerobic microbial degradation of protein and lipid macromolecules in subarctic marine sediment

Claus Pelikan[1,2#], Kenneth Wasmund[1,2#*], Clemens Glombitza[3,4], Bela Hausmann[1,5,6], Craig W. Herbold[1], Mathias Flieder[1], and Alexander Loy[1,2,5*]

[1]*Division of Microbial Ecology, Centre for Microbiology and Environmental Systems Science, University of Vienna, Vienna, Austria.*

[2]*Austrian Polar Research Institute, Vienna, Austria.*

[3]*Center for Geomicrobiology, Department of Biology, Aarhus University, Aarhus, Denmark.*

[4]*ETH Zürich, Department of Environmental Systems Science, Zürich, Switzerland.*

[5]*Joint Microbiome Facility of the Medical University of Vienna and the University of Vienna, Vienna, Austria*

[6]*Department of Laboratory Medicine, Medical University of Vienna, Vienna, Austria*

[#]Contributed equally.

*Correspondence: Kenneth Wasmund (kenneth.wasmund@univie.ac.at) and Alexander Loy (alexander.loy@univie.ac.at)

Running Head: Protein- and lipid-degraders in subarctic marine sediments.

Abstract

Microorganisms in marine sediments play major roles in marine biogeochemical cycles by mineralizing substantial quantities of organic matter from decaying cells. Proteins and lipids are abundant components of necromass, yet microorganisms that degrade them remain understudied. Here, we revealed identities, trophic interactions and genomic features of microorganisms that degraded ^{13}C-labelled proteins and lipids in cold anoxic microcosms with sulfidic subarctic marine sediment. Supplemented proteins and lipids were rapidly fermented to various volatile fatty acids within five days. DNA-stable isotope probing (SIP) suggested *Psychrilyobacter atlanticus* was an important primary degrader of proteins, and *Psychromonas* members were important primary degraders of both proteins and lipids. Closely related *Psychromonas* populations, as represented by distinct 16S rRNA gene variants, differentially utilized either proteins or lipids. DNA-SIP also showed ^{13}C-labeling of various *Deltaproteobacteria* within ten days, indicating trophic transfer of carbon to putative sulfate-reducers. Metagenome-assembled genomes revealed the primary hydrolyzers encoded secreted peptidases or lipases, and enzymes for catabolism of protein or lipid degradation products. *Psychromonas* were prevalent in diverse marine sediments, suggesting they are important players in organic carbon processing *in situ*. Together, this study provides an improved understanding of the metabolic processes and functional partitioning of necromass macromolecules among microorganisms in the seafloor.

53 ## Introduction

54 The majority of marine sediments that underlie the Earth's oceans are dominated by
55 microorganisms mediating heterotrophic processes, which are primarily sustained by “pelagic-
56 benthic” coupling [1]. This is driven by a constant supply of organic matter from planktonic
57 organisms that thrive in the overlying water column and settle with particulate aggregates to the
58 seafloor after their death [2]. The amount and composition of organic matter that reaches the
59 seafloor is strongly dependent on water depth, whereby continental shelves and shallow
60 sediments generally receive greater inputs compared to deep sea sediments [3]. In cold polar
61 regions with lower microbial activities in the water column [4], a large fraction of the phytodetritus
62 from spring bloom-like events reaches the underlying sediments [5]. Additionally, organic matter
63 can originate from autochthonous microbial production [6] and from land-derived sources, which
64 can be substantial in areas close to land and rivers, as well as polar regions subjected to melting
65 [2, 7].
66
67 Organic matter in marine sediments is composed of an immense diversity of
68 macromolecules, of which a substantial fraction can be enzymatically degraded and utilised as
69 nutrient and energy sources by microorganisms [2]. Proteins and lipids typically constitute 10%
70 and 5–10% of the organic matter found in marine sediments, respectively [8, 9]. Proteins, peptides
71 and amino acids are important sources of nitrogen [10], particularly in sediment habitats with
72 limited inorganic nitrogen sources [11]. Lipids generally consist of an alkyl chain that is ester- or
73 ether-bound to a polar head group such as phospho-glycerol, or a glycerol that is glycosidically
74 bound to a sugar moiety. They are major components of phytoplankton biomass [12, 13], of which
75 the less labile fraction survives degradation in the water column [14] and is degraded by
76 microorganisms in the underlying sediments [15]. Long-chain fatty acids released from lipid
77 hydrolysis are energy-rich compounds [16], and can be expected to be favourable substrates for
78 microorganisms.
79

80 Most macromolecules are too large to be directly imported into cells and must therefore
81 be degraded, at least partially, outside the cells [17]. Hydrolysis of macromolecules via the activity
82 of extracellular enzymes is the rate limiting step during organic matter mineralization in
83 heterotrophic marine sediments [17, 18]. Microorganisms utilize a compositionally and
84 functionally large diversity of extracellular hydrolases to facilitate the extracellular breakdown of
85 macromolecules [19]. For example, peptidases in sediments of Arctic fjords in Svalbard had
86 greater substrate ranges for different peptides and much higher activities (tens to hundreds of
87 thousands nmol l^{-1} hr^{-1}) than peptidases in the water column [20]. This showed that sediments act
88 as important biogeochemical hotspots for processing organic macromolecules. Interestingly,
89 peptidase activity was negatively correlated to amounts of phyto-detritus inputs, whereas lipase
90 activity was positively correlated [11]. This indicated that peptidases are excreted in times of
91 nutrient limitation, whereas lipases are excreted when organic matter availability is high [11].
92
93 The microbial degradation of organic macromolecules in anoxic marine sediments is a
94 complex inter-species process involving 'primary degraders' that break down larger
95 macromolecules into oligomers and monomers for fermentation to alcohols, lactate and/or short-
96 chain volatile fatty acids (VFAs), which are then mineralized to CH_4, CO_2 and/or H_2 [21]. 'Terminal
97 oxidizers' of fermentation products prevalent in marine sediments, such as sulfate-reducing
98 microorganisms (SRM), have been relatively well studied [22–27]. On the other hand, the key
99 microbial players responsible for the primary hydrolysis of different types of organic matter and
100 macromolecules are poorly understood. Most studies are based on predictions from genomic
101 analyses [28–31], whereas experimental evidence linking identities to functions are lacking.
102
103 In the present study, we investigated the identities, genomic features, and ecological
104 interactions of microbial taxa that may play important roles in protein and lipid macromolecule
105 degradation in subarctic marine sediments. We performed laboratory experiments whereby
106 sulfidic arctic marine sediments were incubated in microcosms under cold (4 °C), anoxic
107 conditions and supplemented with either ^{13}C-labelled proteins or ^{13}C-labelled lipids. The cold
108 conditions represented large depth expanses of the oceans and seafloor that are permanently

109 cold [32]. These microcosms were also incubated under conditions where sulfate reduction was
110 specifically inhibited, in order to elucidate the roles of SRM. Catabolism and assimilation of ^{13}C-
111 labelled substrates by the sediment microorganisms was investigated by DNA-based stable
112 isotope probing (DNA-SIP) and amplicon sequencing of 16S rRNA genes. The degradation of
113 organic matter was monitored by measuring concentrations of VFAs and sulfate. Genome-
114 resolved metagenomic analyses were used to predict secreted hydrolytic enzymes and
115 reconstruct organic matter degradation pathways encoded by the taxa identified by DNA-SIP.
116 This revealed (i) the identities and foraging strategies of several key protein- and lipid-consuming
117 bacteria in marine sediments, (ii) that niche partitioning among *Psychromonas* subspecies was
118 based on differential utilization of proteins and lipids, and (iii) and that SRM of the family
119 *Desulfobacteraceae* mainly utilized the macromolecule degradation intermediates, i.e., volatile
120 fatty acids.
121

122 ## Materials and methods

123 ***Sediment incubations***

124 Sediment slurries were produced with sediment (0–30 cm below seafloor) from Greenland
125 (Nuuk fjord 'station 3', water depth 498 m, August 2013, 64°26′45″N, 52°47′39″W) mixed 1:1 (v/v)
126 with anoxic artificial seawater [33] containing approximately 28 mM sulfate. For each microcosm,
127 40 ml of this slurry was distributed into 250 ml serum vials under anoxic conditions in an anoxic
128 glove-box (nitrogen atmosphere containing approximately 2% hydrogen and 10% CO_2).
129 Microcosms were sealed with thick rubber stoppers and crimped, and flushed with N_2 after
130 removing from the anoxic glove-box. All subsequent subsampling was also performed within the
131 anoxic glove-box, with microcosms placed on ice-packs to minimize warming of incubations.
132 Triplicate microcosms were either supplemented with a single dose of: i) 300 µg C g^{-1} ^{13}C-labelled
133 Algal lipid mixture-99 atom% ^{13}C (ISOTEC, Sigma-Aldrich); ii) 300 µg C g^{-1} ^{13}C-labelled Algal
134 crude protein extract-98 atom% ^{13}C (ISOTEC, Sigma-Aldrich), iii) 300 µg C g^{-1} ^{13}C-labelled Algal
135 lipid mixture (as above) and the sulfate reduction inhibitor molybdate (28 mM; [34]); v) 300 µg C
136 g^{-1} ^{13}C-labelled Algal protein mixture (as above) and molybdate (28 mM); or v) were left without

137 supplementation (no-substrate controls). The microcosms were incubated at 4 °C and were
138 sampled after 2, 5, 10, 17, 25 and 48 days of incubation. Sediment slurry samples were taken for
139 analysis of volatile fatty acids and sulfate (1 ml), as well as for DNA-based analyses (0.5 ml).
140 Samples were stored on pre-cooled ice packs in the anoxic glove box and were transferred
141 immediately to the –80 °C freezer after sampling. Sampling, processing and molecular biological
142 analyses of sediment samples from Svalbard, Norway, are presented as Supplementary
143 information.
144
145 ***Determination of sulfate and volatile fatty acid concentrations***
146 Sulfate concentrations in interstitial water samples of microcosms were determined by
147 capillary electrophoresis (P/ACETM MDQ molecular characterization system, Beckman Coulter)
148 with the CEofixTM anions 5 kit (Analis). Standards were produced by dissolving known
149 concentrations of Na_2SO_4 in artificial seawater. The concentrations of VFAs were determined as
150 follows: samples were defrosted, vortexed and centrifuged at 10 000 rpm for 10 minutes. 100 µl
151 of the supernatant was diluted 1:10 (v/v) in Milli-Q water. Syringe filters (Acrodisc IC grade filter,
152 d=13 mm, Suprapor® membrane with 0.2 µm pore size) were first rinsed with 10 ml Milli-Q water
153 followed by 0.5 ml of diluted sample to minimize further dilution with the rinsing water. Another
154 0.5 ml of sample were then filtered and measured by 2-dimensional ion chromatography-mass
155 spectrometry (IC-IC-MS; Dionex ICS-3000 coupled to an MSQ Plus™, both Thermo Scientific),
156 equipped with an Ion Pack™ AS 24 as the first column to separate bulk VFAs from chloride, and
157 an Ion Pack™ AS 11 HC as the second column to separate individual VFAs [35].
158
159 ***DNA extraction***
160 For DNA-SIP gradients and PCR-based amplicon sequencing, DNA was extracted using
161 a combination of bead beating, cetyltrimethylammonium bromide-containing buffer and phenol-
162 chloroform extractions. Sediment slurry (0.5 ml) was added to Lysing Matrix E tubes (MP
163 Biomedicals) and were suspended in 0.675 ml cetyltrimethylammonium bromide containing
164 extraction buffer, as described previously [36]. The tubes were placed on a rotary shaker (200
165 rpm) and incubated at 37 °C for 30 minutes. The samples were supplemented with 75 µL of

166 sodium dodecyl sulfate (20% w/v) and were then incubated for 1 hour at 65 °C (tubes were
167 inverted every 20 minutes). Samples were subjected to two rounds of bead beating with a speed
168 setting 6 for 30 s using a FastPrep®-24 bead beater (MP Biomedicals). In between the beat
169 beating steps, samples were cooled on ice. Debris was pelleted by centrifugation at 6000 g for 10
170 minutes at 25 °C and supernatant was collected. An equal volume of phenol:chloroform:isoamyl
171 (25:24:1) alcohol (ROTH) was added to the supernatant and tubes were repeatedly inverted,
172 followed by centrifugation at 16 000 g for 10 min at 25 °C. The aqueous phase (upper layer) was
173 transferred into a clean 1.5 ml tube, supplemented with 0.6 volume of 2-propanol and incubated
174 for 1 hour at 4 °C to precipitate DNA. The precipitate was then pelleted by centrifugation at 16
175 000 g for 30 min at 4 °C. DNA pellets were washed with 250 µL of 70% (v/v) ethanol, air-dried
176 and resuspended in 50 µL Tris buffer [10 mM Tris-HCl (pH 8.0)]. For metagenome sequencing,
177 DNA was extracted from day 0 and from individual sediment microcosm samples at days 5, 17
178 and 25 (for both protein and lipid amended treatments) using the Ultra Pure Power Soil Kit (MoBio)
179 and following manufacturers' protocol.
180
181 ***DNA-SIP gradients***
182 CsCl gradients with 5 µg DNA were prepared in a temperature controlled room at 23 °C
183 according to a previously published protocol [37]. The gradient mixtures were added to
184 ultracentrifuge tubes (Beckman Coulter) and were centrifuged in an Optima L-100XP
185 ultracentrifuge (Beckman Coulter) using the VTi 90 rotor for >48 hours at 146286 rcf (44100 rpm)
186 at 20 °C. After centrifugation, gradients were fractionated into 250 µl fractions by puncturing the
187 bottom of the tube with a sterile needle and adding water to the gradient tube at the top using a
188 sterile needle and a syringe pump (World Precision Instruments). The density of collected
189 fractions was determined by using a digital refractometer (AR 200, Reichert Analytical Instrument)
190 at 23 °C. The DNA-SIP fractions were considered heavy at densities >1.726 g ml^{-1} and light at
191 densities <1.720 g ml^{-1} (Supplementary Figure S1). Afterwards, DNA was precipitated with 500
192 µL sterile PEG 6000 (30% polyethylene glycol 6000 and 1.6 M NaCl) and 1 µL of glycogen (5 µg
193 ml^{-1}) and subsequently purified as described previously [37]. Bacterial DNA in SIP fractions was
194 quantified by quantitative PCR (qPCR) using the primers 341F 5′-CCT ACG GGA GGC AGC AG-

195 3′ and 534R 5′-ATT ACG GCG GCT GCT GGC A-3′. The 20 µL qPCR mix contained 1× IQ™
196 SYBR Green Supermix (BIO-RAD), 0.25 µM of each primer and 1 µL of 1:10 diluted DNA from
197 individual gradient fractions. The program used for thermal cycling on the iCycler thermal cycler
198 (Bio-Rad) consisted of: 3 min at 95 °C, followed by 39 cycles of 95 °C for 15 s, 60 °C for 30 s and
199 72 °C for 39 s, and was followed by a melting curve from 60 °C to 95 °C by increments of 0.5 °C
200 every 5 s.
201
202 ***Amplicon sequencing and analysis***
203 Barcoded 16S rRNA gene amplicons for Illumina MiSeq sequencing were produced using
204 a previously established two-step PCR approach [38, 39]. Raw reads were processed as
205 described previously [38, 39]. The identity threshold used for OTU clustering was 97% identity.
206 Sub-OTU diversity at single-nucleotide resolution in the amplicon data was investigated using
207 cluster-free filtering [40]. Statistical significance of differences in OTU relative abundances
208 between treatments was determined using DESeq2 (version 1.10.1) [41] in the R software
209 environment (R core team, 2019). Additionally, an OTU was considered to be ^{13}C-enriched when
210 it was significantly more abundant in heavy SIP fractions compared to light fractions obtained
211 from the same incubation [42], which was also determined using DESeq2. The sequence
212 abundance of each OTU in the 'heavy' part (>1.726 g ml^{-1}) of the DNA-SIP gradient (numerator)
213 were compared to sequence abundance in the 'light' part (<1.720 g ml^{-1}) of the DNA-SIP gradient
214 (denominator). Specific samples used for comparisons are indicated in Supplementary Figure S1.
215 Only OTUs with more than 5 reads in 5 out of all 32 samples from gradient fractions were
216 considered during DESeq2 analyses. Results were extracted with the command:
217 `results(cooksCutoff = FALSE, altHypothesis = "greater")`
218 and were considered statistically significant if: (i) the false-discovery-rate (FDR)-adjusted p-value
219 was below 0.1, and (ii) the respective OTU was not significantly enriched in the heavy fractions
220 of the DNA-SIP gradient from the no-substrate incubations. OTU counts were 'rlog' transformed
221 with DESeq2 and heatmaps of enriched OTUs were created with R software package pheatmap
222 (version 1.0.8).

223 The presence of 16S rRNA gene sequences related (>97% identity) to specific organisms
224 of interest in publicly available amplicon-derived datasets were determined using the IMNGS
225 server [43], with 100 bp overlap as minimum.
226
227 ***Metagenome sequencing and differential coverage binning***
228 Metagenome libraries were produced with the Nextera XT DNA Library Preparation Kit
229 (Illumina) and sequencing was performed at the Vienna Biocenter Core Facilities Next Generation
230 Sequencing facility (Vienna, Austria) on an Illumina Hiseq 2500 using HiSeq V4 chemistry with
231 the 125 bp paired-end mode. Reads were end trimmed at the first base with a q-score below 10
232 and reads with less than 50 bp were removed. For assembly, sequence coverage was normalized
233 across samples using bbnorm with an average read depth of 100 and a minimum read depth of
234 3 (BBmap version 33.57 http://sourceforge.net/projects/bbmap/). Normalized read files were
235 assembled with IDBA-UD [44] and SPAdes [45] using default parameters. Reads of each sample
236 (non-normalized) were mapped to each assembly using BWA [46], and coverage information was
237 obtained using SAMtools [47]. Differential coverage binning was performed with MetaBAT [48],
238 MaxBin [49], and CONCOCT [50]. Following the binning programs default parameters, only
239 contigs with a minimum length of 2500 and 1000 bp were used for binning with MetaBAT and
240 MaxBin/CONCOCT, respectively. The resulting metagenome-assembled genomes (MAGs)
241 generated from different assemblies and binning programs were aggregated with DASTool [51],
242 and de-replicated with dRep using default parameters [52]. MAGs that could be linked to ^{13}C-
243 incorporating OTUs during protein and lipid hydrolysis by 16S rRNA gene sequence identity were
244 further analysed. Selected MAGs were evaluated for completion and contamination using
245 CheckM [53], and classified using the Genome Taxonomy Database (GTDB) release 86 [54] and
246 GTDB-Tk version 0.1.3 [55]. A genome-based phylogenetic analysis of MAGs, the genome of the
247 type strain *Psychrilyobacter atlanticus* HAW-EB21 and closely related reference genomes, was
248 constructed from the concatenated marker protein alignment produced by CheckM [53]. The
249 phylogenetic tree was built from this concatenated marker alignment with IQ-TREE using
250 automatic substitution model selection (LG+F+I+G4) [56] and ultrafast bootstrap approximation
251 with 1000 replicates [57]. The tree was visualized with iTOL [58]. Average nucleotide identities

252 (ANI) and average amino acid identities (AAI) of selected MAGs and closely related reference
253 genomes were determined using all-vs-all FastANI 1.1 with default parameters [59] and
254 CompareM 0.0.23 (aai_wf) with default parameters (https://github.com/dparks1134/CompareM),
255 respectively.
256
257 ***Genome annotation***
258 MAGs were annotated with the MicroScope annotation platform [60] and using the RAST
259 server [61]. The annotations of proteins were confirmed by DIAMOND searches [62] against the
260 NCBI-nr database (e-value 10^{-5}), hidden Markov model-based searches using InterProScan [63]
261 with the databases Pfam-A [64] and TIGRFAM [65], and online BLASTP searches against the
262 UniProt database [66]. Possible hydrolytic enzymes were examined for signal peptide sequences
263 that facilitate secretion from the cytoplasm and transmembrane helices using the Phobius online
264 server [67] and using PSORTb version 3.0 [68]. Furthermore, peptidases, lipases/esterases and
265 glycoside hydrolases were additionally compared to the databases MEROPS [69], ESTHER [70]
266 and CAZY [71], respectively, using DIAMOND searches (e-value $>10^{-5}$, identity ≥30%). Further,
267 searches were made against the NCBI-nr database using BLASTP [72] for certain proteins of
268 interest. The selection of potentially catabolic peptidases encoded by genomes and MAGs was
269 based on two recent studies about extracellular peptidases in marine sediments [29, 73]. In
270 addition, non-peptidase homologs and peptidases with regulatory functions, e.g., peptidases
271 involved in membrane protein remodelling, as indicated by MEROPS database descriptions, were
272 not considered (Supplementary Table S1). Potentially catabolic lipases/esterases were selected
273 based on the ESTHER database descriptions (Supplementary Table S1).
274
275 ***Phylogenetic analyses of 16S rRNA gene sequences***
276 16S rRNA gene sequences were aligned and classified with the SINA aligner [74], using
277 the SILVA database release 128 [75]. Full-length sequences of close relatives of 16S rRNA OTUs
278 were extracted from the SILVA database and combined with the aligned 16S rRNA genes
279 sequences that were obtained from MAGs. A reference tree was then constructed using FastTree

280 [76]. Subsequently, 16S rRNA OTUS and partial 16S rRNA genes from MAGs were added to the
281 reference tree using the EPA algorithm [77] in RAxML [78]. Trees were visualized in iTOL [58].
282
283 ***Statistical analyses***
284 Statistics for comparisons of VFAs and sulfate in treatment series versus controls were
285 determined with Student's T tests using the function t.test() in the R software environment (R core
286 team, 2014).
287
288 ***Data availability***
289 All sequence datasets and metagenome-assembled genomes from the DNA-SIP
290 experiments are available under the NCBI-Genbank Bioproject PRJNA609450. DNA-SIP
291 amplicon sequencing datasets are available in the NCBI-Genbank Sequence Read Archive under
292 BioSample accession SAMN14253696 and SRA accessions SRR11221408-SRR11221561.
293 Metagenomic sequence reads are available in the NCBI-Genbank Sequence Read Archive under
294 BioSample accession numbers SAMN14421543–SAMN14421548. Metagenome-assembled
295 genomes are available in the NCBI-Genbank under BioSample accession numbers
296 SAMN14421524-SAMN14421532. Annotated MAGs and genomes from the MicroScope
297 annotation platform for key protein- and lipid-degrading organisms, and *Psychrilyobacter*
298 *atlanticus* DSM 19335, are publicly available in the MaGe-Microscope server
299 (https://mage.genoscope.cns.fr/). Amplicon sequencing datasets from Svalbard sediments are
300 available under NCBI-Genbank Bioproject PRJNA623111 and the BioSample accession numbers
301 SAMN14538997-SAMN14539076.
302
303 **Results**
304 ***Sulfate removal and volatile fatty acid turnover during protein and lipid degradation***
305 Sulfate was largely turned-over after 48 days in all incubation treatments (down to 0.6–
306 2.4 mM), except in incubations where sulfate reduction was inhibited by molybdate, where it
307 remained between 18.1–24.2 mM (Figure 1A). Sulfate turnover was fastest between days 5 and

308 25, and was stimulated by the additions of proteins or lipids. Of all measured VFAs, acetate was
309 the most prominent, reaching concentrations of over 900 μM in protein amended microcosms on
310 day 17. Formation of the next most abundant VFA, formate, peaked at around 50 μM in
311 lipid/molybdate-amended microcosms. Supplementation of proteins to the incubations resulted in
312 significantly higher concentrations of acetate from days 2–5 compared to no-substrate controls
313 (Supplementary Table S2). While the stimulation of acetate production from lipid additions was
314 noticeably more than in no-substrate controls, the differences were not statistically significant
315 (Supplementary Table S2). Significantly more propionate, butyrate and isobutyrate were
316 produced in protein- and lipid-amended microcosms, as compared to the no-substrate controls
317 (mainly between 2–5 days) (Figure 1B, Supplementary Table S2). Molybdate-inhibited
318 incubations supplemented with proteins or lipids showed increased accumulation of formate,
319 butyrate, and isobutyrate, but decreased production of acetate and propionate.
320
321 ***^{13}C-labeling of OTUs and sub-OTUs during protein and lipid degradation***
322 To evaluate incorporation of ^{13}C from the added ^{13}C-labelled proteins or lipids into the DNA
323 of microorganisms, bacterial 16S rRNA genes were quantified by qPCR across individual SIP
324 fractions (Supplementary Figure S1). Higher relative copy numbers were detected in the 'heavy'
325 fractions of the gradients (i.e., densities >1.726 g ml^{-1}) from both ^{13}C-protein and ^{13}C-lipid
326 incubations relative to corresponding no-substrate controls at days 5 and 10. This indicated ^{13}C-
327 uptake and incorporation into DNA at these early time points. At days 17 and 25, only very small
328 or no differences in relative 16S rRNA gene copy numbers between gradients from the ^{13}C-
329 substrate incubations and the no-substrate control incubations were observed.
330
331 Microbial community analysis of SIP fractions by 16S rRNA gene amplicon sequencing
332 identified five OTUs (Clostridia-JTB215 OTU 1, *Psychromonas* OTU 4, *Psychrilyobacter* OTU 5,
333 *Fusibacter* OTU 38 and *Photobacterium* OTU 54) that were significantly enriched in heavy SIP
334 fractions from the ^{13}C-protein incubations at day 5 (Figure 2A; Supplementary Table S3). At day
335 10, another 19 OTUs were significantly enriched in heavy SIP fractions from incubations with ^{13}C-
336 protein amendments (Figure 2A). These were affiliated with the classes *Deltaproteobacteria*

337 (OTUs 2, 19, 36, 44, 67, 183, 232, 892, 4719), *Gammaproteobacteria* (OTUs 80, 128, 205, 285)
338 and the phyla *Bacteroidetes* (OTUs 124 and 184), *Firmicutes* (OTUs 202 and 4050) and
339 *Marinimicrobia* (OTU 123), or were unclassified (OTU 312) (Supplementary Figure S2).
340
341 In SIP gradients from ^{13}C-lipid amended incubations at day 5, significant ^{13}C-enrichment
342 was revealed for only two gammaproteobacterial OTUs, i.e., *Psychromonas* OTU 4 and *Vibrio*
343 OTU 80 (Figure 2A). An analysis of the microdiversity within *Psychromonas* OTU 4 identified four
344 *Psychromonas* sub-OTUs (sub-OTUs 4, 192, 9 and 42) that responded differently in incubations
345 with protein or lipid amendments. The sub-OTUs 4 and 192 were significantly enriched in heavy
346 fractions of ^{13}C-lipid incubations (Figure 3A) and were more closely related to each other than to
347 sub-OTUs 9 and 43 (Figure 3B). Furthermore, the relative abundance of sub-OTUs 4 and 192
348 increased in the microcosms from ^{13}C-lipid incubations compared to no-substrate control
349 microcosms (Figure 3C). In contrast, the sub-OTUs 9 and 43 were significantly enriched in heavy
350 SIP fractions from ^{13}C-protein incubations, and sub-OTU 9 increased in relative abundance in the
351 microcosms from ^{13}C-protein incubations compared to no-substrate control microcosms (Figure
352 3C). No sub-OTU microdiversity was detected in any other OTU that was significantly enriched in
353 ^{13}C. At day 10, we identified three additional OTUs enriched in the heavy SIP fractions from ^{13}C-
354 lipid incubations that were affiliated with the phylum *Firmicutes* (OTUs 1 and 4141) and the class
355 *Deltaproteobacteria* (OTU 13310) (Figure 2A).
356
357 We also compared the relative abundances of 16S rRNA OTUs among the protein- or
358 lipid-amended microcosms versus no-substrate control microcosms over time. Here, we restricted
359 the analysis to OTUs (n=26) that were enriched in ^{13}C from the protein- and lipid-amended
360 treatments (described above). Between days 5 and 10, ten OTUs (1, 2, 4, 5, 19, 54, 80, 285, 4141
361 and 13310) significantly increased in relative abundances in substrate-amended incubations as
362 compared to the no-substrate controls (Supplementary Figure S3A and Supplementary Table
363 S2). Most notably, several OTUs showed relatively large differences in relative abundances
364 between amended and no-substrate controls, and consequently had high relative abundances
365 among the overall communities. For instance, *Psychrilyobacter* OTU 5 reached relative

366 abundances of around 9–10% after 2–5 days in protein-amended microcosms, while staying
367 around 3–4% in no-substrate controls. *Psychromonas* OTU 4 reached relative abundances of
368 around 15–16% between 5–10 days after lipid amendments, while also reaching around 5–7% in
369 the protein-amended microcosms from days 2–10. In contrast, *Psychromonas* OTU 4 stayed
370 below 2.5% in the no-substrate controls over-time. The relatively fast (<10 days) and clear
371 increases in relative abundances of these OTUs due to substrate additions therefore provided
372 evidence for their direct involvement in substrate utilization for growth. On the contrary, the
373 Clostridia-JTB215 OTU 1 also showed large increases in relative abundances from both protein-
374 and lipid-amendments versus no-substrate controls, however, the response was relatively
375 delayed, i.e., such increases developed mainly after 10 days.
376
377 Relative abundances of OTUs 1, 2, 67, 4050 and 4141 were significantly lower in
378 microcosms with the sulfate-reduction-inhibitor molybdate than in microcosms without molybdate.
379 This suggests that these OTUs are SRM or dependent on SRM activity.
380
381 ***Genomic evidence for extracellular hydrolysis of proteins and lipids***
382 Samples from day 0, and from days 5, 17 and 25 from the lipid- and protein-amended
383 microcosms were selected for metagenome sequencing. The aim was to recover genomes of
384 organisms that were ^{13}C-labelled from protein or lipid treatments, and to specifically analyse their
385 catabolic potentials for these macromolecules. Overall, nine metagenome-assembled genomes
386 (MAGs) were recovered with >80% completeness and <5% contamination. Two had 16S rRNA
387 sequences identical to bacterial OTUs that incorporated ^{13}C from protein or lipid hydrolysis, i.e.,
388 *Psychromonas* MAG GLG-1 and *Clostridia* MAG GPF-1 (Supplementary Figure S2). All MAGs
389 that were affiliated with the genus *Psychrilyobacter* were very incomplete (<20%) (data not
390 shown). Therefore, we analysed the publicly available genome of the type strain *Psychrilyobacter*
391 *atlanticus* HAW-EB21. This strain was isolated from marine sediments [79], and had a 16S rRNA
392 sequence that was identical to *Psychrilyobacter* OTU 5 that was labelled from protein
393 amendments (Supplementary Figure S2). A *Desulfoluna* MAG GLD-1 was also analysed in detail
394 because it encoded potential to degrade VFAs and/or lipids, although it could not be confidently

395 linked to any 16S rRNA OTU sequences and it is therefore presented in the Supplementary
396 results.
397
398 *Psychromonas* MAG GLG-1 was most closely related to *Psychromonas aquimarina* ATCC
399 BAA-1526 (ANI 80.7% of 41.8% aligned) (Supplementary Table S4) and encoded a 16S rRNA
400 sequence that was identical to *Psychromonas* sub-OTU 4 (Supplementary Figure S2). *Clostridia*
401 MAG GPF-1 was only distantly related to any publicly available genome (Supplementary Figure
402 S4), with an AAI of only 53.4% (of 37% aligned) (ANI was too low to calculate) to the most-related
403 genome of *Caloranaerobacter azorensis* DSM 13643 (Supplementary Table S4). A short 16S
404 rRNA fragment (92 bp) was retrieved from *Clostridia* MAG GPF-1 and was linked to the 16S rRNA
405 OTU 1 by phylogenetic placement into a reference tree (Supplementary Figure S2). The
406 genomes/MAGs of putative protein and/or lipid-degraders were subsequently analysed for
407 encoded capabilities to degrade proteins (*P. atlanticus* corresponding to 16S rRNA OTU 5), lipids
408 (*Psychromonas* MAG GLG-1 corresponding to sub-OTU 4) or both macromolecules (*Clostridia*
409 MAG GPF-1 corresponding to 16S rRNA OTU 1).
410
411 The genome of *Psychrilyobacter atlanticus* HAW-EB21 encodes a variety of peptidases
412 (*n*=24), which were likely involved in the breakdown of peptides for further catabolism of amino
413 acids (Supplementary Table S5). Two of these peptidases (i.e., M3 and M24) encoded signal
414 peptides for translocation across the cytoplasmic membrane (Figure 4). Overall, the genome of
415 *P. atlanticus* encodes an array of predicted peptide (*n*=19) and amino acid transporters (*n*=38),
416 especially when compared to the MAGs of the putative lipid degraders *Psychromonas* MAG GLG-
417 1 (peptide transporter, *n*=6; amino acid transporter, *n*=14) (Supplementary Table S5).
418 Furthermore, the genome of *P. atlanticus* encoded for proton-dependent peptide transportation
419 (Supplementary Table S5).
420
421 The lipid-metabolizing capability of *Psychromonas* MAG GLG-1 was supported by the
422 presence of genes for an extracellular phospholipase D/alkaline phosphatase and a
423 carboxylesterase with a signal peptide sequence, which corresponded to the ESTHER family

424 Carboxylesterase type-B (Supplementary Table S5). The long chain fatty acids that resulted from
425 extracellular degradation of acyl chain esters were likely taken-up by cells via two predicted long-
426 chain fatty acid transporters (Supplementary Table S5). Predicted glycerol transporters were not
427 encoded in the genome of *Psychromonas* MAG GLG-1. Because our study revealed
428 *Psychromonas* spp. to be potentially important lipid and protein degraders, we also investigated
429 available genomes and/or MAGs (*n*=16) from publicly available databases in order to examine
430 the prevalence of the encoded capacity to utilize extracellular proteins or lipids via extracellular
431 hydrolases (Supplementary Table S6). This identified predicted secreted phospholipases in most
432 genomes (*n*=10), while predicted secreted proteases/peptidases were restricted to 4 genomes
433 (Supplementary Figure S6).
434
435 *Clostridia* MAG GPF-1 encoded the largest number of peptidases (*n*=29) of all analysed
436 MAGs/genomes (Supplementary Table S5). Three of these peptidases (M20, M24 and S8
437 peptidase families) have predicted secretion signal peptides and might be excreted to the
438 extracellular space via the SEC pathway (Figure 4). Similar to *P. atlanticus*, *Clostridia* MAG GPF-
439 1 encoded a broad array of predicted peptide (*n*=14) and amino acid (*n*=24) transporters. In
440 accordance with the DNA-SIP results, *Clostridia* MAG GPF-1 also has the potential for catabolic
441 breakdown of lipids. The MAG encoded one potentially secreted catabolic esterase/lipase that
442 correspond to the ESTHER family Bacterial_EstLip_FamX, and two predicted membrane-bound
443 esterases/lipases that correspond to the ESTHER families Bacterial_EstLip_Fam and
444 Carboxylesterase, type B (Supplementary Table S5). The presence of genes for
445 esterases/lipases in the genome of *Clostridia* MAG GPF-1 indicated the potential of this MAG to
446 hydrolyse ester bonds between glycerol and fatty acids. Because genes encoding for known fatty
447 acid transport and catabolism were absent from the genome of *Clostridia* MAG GPF-1, this
448 bacterium might instead utilize glycerol. This was supported by an encoded glycerol-3-phosphate
449 transporter and a putative glycerol facilitator protein, which were also encoded directly adjacent
450 to a glycerol kinase, which catalyses the first step of the cytoplasmic catabolism of this substrate
451 (Supplementary Table S5).
452

453 ***Intracellular catabolism of protein and lipid degradation intermediates***

454 The genome of *P. atlanticus* encoded 22 cytoplasmic peptidases with possible catabolic
455 roles (Supplementary Table S5). In comparison, the genomes of the putative lipid degrader, i.e.,
456 *Psychromonas* MAG GLG-1 encoded only 7 intracellular peptidases. In this study, we focused on
457 amino acid degradation processes that form glutamate and/or keto-acids for central carbon
458 metabolism and that could therefore explain incorporation of ^{13}C-carbon from the ^{13}C-labelled
459 proteins into DNA, as well as the development of VFAs in our incubations (Figure 4). The genome
460 of *P. atlanticus* encoded several aminotransferases and other amino acid degrading enzymes
461 (i.e., alanine dehydrogenases, cystathionine gamma-lyase, serine/threonine ammonia-lyase,
462 tryptophanase and methionine gamma-lyase) (Supplementary Table S5). These can convert
463 amino acids to the keto-acids pyruvate and oxobutanoate, which could then be fermented to
464 formate, and either acetate or propionate, respectively (Figure 4).

465

466 *Psychromonas* MAG GLG-1 encoded all enzymes required for beta-oxidation of fatty
467 acids, including a putative multienzyme complex that contains the two enzymes enoyl-CoA
468 hydratase/isomerase and 3-hydroxyacyl-CoA dehydrogenase (Supplementary Table S5).
469 Through beta-oxidation, even- and odd-chain fatty acids can be converted to propionyl- and
470 acetyl-CoA, which can be further fermented to acetate and propionate, respectively (Figure 4). In
471 comparison to *P. atlanticus* and *Clostridia* MAG GPF-1, which encoded strict fermentative
472 metabolisms, *Psychromonas* MAG GLG-1 also encoded a complete oxidative TCA cycle, which
473 enables a respiratory conversion of acetyl-CoA to CO_2 (Figure 4). When oxygen is available,
474 *Psychromonas* MAG GLG-1 might use one of the two encoded high affinity oxidases for
475 respiration, i.e., cbb3-type cytochrome *c* oxidase and cytochrome *bd*–type oxidase
476 (Supplementary Table S5). In oxygen-depleted sediments like in our microcosm incubations,
477 *Psychromonas* GLG-1 might ferment, or may respire using nitrate (dissimilatory nitrate reduction
478 to ammonium, DNRA) or fumarate as terminal electron acceptors (Supplementary Table S5).
479 Genes necessary for the intracellular degradation of glycerol were absent from *Psychromonas*
480 MAG GLG-1 (Supplementary Table S5). Furthermore, despite the presence of genes for several
481 extracellular glycosyl hydrolases in the genome of *Psychromonas* MAG GLG-1 and a complete

482 glycolysis pathway (Supplementary Table S5), enzymes for feeding galactose or glycerol
483 (subcomponents of Spirulina-derived galactosyl diglycerides), into glycolysis, were not identified.
484
485 The *Clostridia* MAG GPF-1 encoded the largest set of intracellular peptidases (*n*=26) of
486 all investigated genomes (Supplementary Table S5). The fermentation of amino acids by
487 *Clostridia* GPF-1 to propionate, acetate or formate, i.e., via aminotransferases and other amino
488 acid degrading enzymes (i.e., L-threonine 3-dehydrogenase, cystathionine β-synthase,
489 cystathionine gamma-lyase, serine/threonine ammonia-lyase and methionine gamma-lyase) was
490 mostly similar to the predicted routes used by *P. atlanticus*, although genes for lysine fermentation
491 were not present and the glutamate degradation pathways were incomplete (Supplementary
492 Table S5). In addition, the *Clostridia* MAG GPF-1 was the only MAG that encoded enzymes that
493 initiate valine degradation, i.e., two branched-chain amino acid transferases and the gene 2-keto-
494 isovalerate dehydrogenase that is part of the branched-chain α-keto acid dehydrogenase complex
495 (Supplementary Table S5). Besides the potential for amino acid degradation, *Clostridia* MAG
496 GPF-1 also encoded all genes necessary for the conversion of glycerol and glycerol-3-phosphate
497 to pyruvate (Supplementary Table S5), which may help explain with the ^{13}C enrichment of 16S
498 rRNA OTU 1 in ^{13}C-lipid amended incubations (Figure 2).
499
500 ***Environmental distributions of key taxa***
501 To explore fine-scale depth distributions of the main primary-hydrolysing *Psychromonas*
502 and *Psychrilyobacter* species in sulfidic arctic marine sediments, we examined 16S rRNA-gene
503 and -cDNA derived sequence datasets from sediments of Smeerenbergfjord, Svalbard
504 (Supplementary Figure S6). This showed that *Psychromonas* sequences reached 1.7% and 1.9%
505 relative abundances in 16S rRNA-gene and -cDNA libraries in 0–1 centimetres below seafloor
506 (cmbsf) samples from Station GK, respectively. In a nearby core from Station J, they also reached
507 1.2% relative abundances in both 16S rRNA-gene and -cDNA libraries in 0–1 cmbsf samples. At
508 both sites, relative abundances of *Psychromonas* 16S rRNA-genes and -transcripts were very
509 low under 3 cmbsf (Supplementary Figure S6). Sequences from the *Psychrilyobacter* reached
510 only 0.3% in 0–1 cmbsf from Station J samples and comprised maximally only 0.05% of the 16S

511 rRNA transcripts in the same sample (results not shown). *Psychrilyobacter* sequences were under
512 0.03% in all other samples deeper than 1 cmbsf. Further, to gauge their prevalence in other
513 marine sediments, we examined sequences that were similar (>97% identity) to the
514 *Psychromonas* and *Psychrilyobacter* OTUs recovered in this study to sequences in publicly
515 available 16S rRNA gene datasets. This showed that sequences related to these organisms were
516 widely distributed in sediment sites around the worlds oceans (Supplementary Figure S7). For
517 example, *Psychromonas* sequences reached a maximum of 4% relative abundance in seagrass-
518 associated sediments (Nantucket Sound, USA).
519

520 ## Discussion

521 Proteins and lipids comprise a significant fraction (up to 10% each) of organic matter in
522 marine sediments [8, 9], and therefore represent major nutrient and energy sources for sediment
523 microbiomes. Our experiment showed that supplemented proteins and lipids were actively utilized
524 by microorganisms within 5 days of incubation. Both protein and lipid amendments induced rapid
525 accumulation of several VFAs, demonstrating primary fermentation of both macromolecules.
526 DNA-SIP further showed that ^{13}C-carbon from protein and lipid catabolism was incorporated into
527 the DNA of specific taxa within 5 days. This was also paralleled by sharp increases in the relative
528 abundances by many of the same taxa in the corresponding microcosms. We therefore reasoned
529 that taxa that were ^{13}C-labelled and stimulated to higher relative abundances (>1%) within the
530 first 5 days represented the main primary hydrolysers and fermenters of proteins or lipids. Thus,
531 the following discussion especially focuses on these primary hydrolysing taxa.
532

533 Overall, more diverse OTUs incorporated ^{13}C-carbon from proteins compared to lipids,
534 especially after 10 days of incubation, possibly due to a combination of: i) higher proportions and
535 bioavailability of proteins in sediments [8, 9], ii) greater nutritional value of proteins (e.g., nitrogen),
536 and/or iii) a greater biodegradability of proteins as compared to lipids [80]. Sediment
537 microorganisms are also known to efficiently salvage organic nitrogen sources such as amino

538 acids in times of low nutrient supply [11]. Therefore, some microorganisms may have salvaged
539 free peptides or amino acids released from the primary hydrolysers and became ^{13}C-labelled.
540
541 The *Psychromonas* 16S rRNA gene OTU 4 was notable in this study because our DNA-
542 SIP results showed that it was a prominent degrader of both lipids and proteins. Interestingly, we
543 could distinguish four sub-OTUs that each had distinct preferences for either lipids or proteins.
544 Thus, this demonstrated that closely related populations of *Psychromonas* in marine sediments
545 have very different preferences for macromolecules that require completely different catabolic
546 machinery. From the metagenomic analyses, the *Psychromonas* MAG GLG-1, which represented
547 the lipid-degrading sub-OTU 4 population, indeed had gene content that supported its capacity to
548 digest lipids and catabolize fatty acids. For instance, it encoded a secreted esterase/lipase to
549 digest lipids from the extracellular environment, as well as long-chain fatty acid transporters and
550 a beta-oxidation pathway to import and catabolize the fatty acids (Figure 4). Although we did not
551 recover any *Psychromonas* MAGs representative of the protein-degrading populations,
552 comparative genomic analyses of publicly available *Psychromonas* genomes and MAGs showed
553 predicted secreted lipases and/or peptidases are common among this genus. Diverse members
554 of this genus therefore have unique potentials to utilize lipids or proteins.
555
556 Our microbial community profiling showed that *Psychromonas* were relatively abundant
557 and active (based on 16S rRNA expression) in shallow sediments (<3 cmbsf) from arctic Svalbard.
558 *Psychromonas* were previously shown to be highly correlated with fluxes of fresh phyto-detritus
559 to surface sediments of the arctic Laptev Sea [81]. Together with our experimental and genomic
560 analyses, this suggests *Psychromonas* play an active role in the turn-over of 'fresh' and labile
561 organic matter delivered to surface marine sediments from the water column. This is inline with
562 previous experiments that showed *Psychromonas* were important players in the initial degradation
563 of whole Spirulina (cyanobacterial) necromass in arctic marine sediment [23]. Our study therefore
564 suggests that *Psychromonas* populations thrive in surface sediments by utilizing abundant
565 macromolecules that represent fresh and labile organic matter, e.g., lipids and/or proteins.
566

567 We further showed that *Psychrilyobacter* OTU 5 was one of the most prominent protein
568 and/or amino acid degraders in our experiment. Members of this genus were also shown to be
569 important degraders of whole Spirulina necromass in marine sediment experiments [23, 33]. Here,
570 we therefore deciphered their role in bulk organic matter degradation by showing that they are
571 efficient degraders of detrital protein/peptides. Correspondingly, genomic analyses showed that
572 the *Psychrilyobacter atlanticus* type strain HAW-EB21 [79], which had 100% 16S rRNA sequence
573 identity to OTU 5, encoded various routes for the degradation of peptides and for the subsequent
574 fermentation of amino acids (Figure 4) [79]. Their overall contributions to protein degradation in
575 marine sediments may, however, be less than the *Psychromonas* because they were not
576 abundant members of most sedimentary microbiomes analysed.
577
578 The Clostridia MAG GPF-1 (16S rRNA-OTU 1), had less than 54% AAI to any available
579 genome, and therefore our data represents the first insights into the potential metabolism of this
580 uncultured group. Overall, our analyses suggested these organisms are versatile nutrient utilizers.
581 The Clostridia OTU 1 population was ^{13}C-labelled in SIP analyses from both ^{13}C-protein and -lipid
582 incubations, and its relative abundances were also boosted by the additions of both substrates,
583 although to a much lesser extent than the *Psychromonas* or *Psychrilyobacter*. Our genomic
584 analyses indicated the potential to utilize peptides, amino acids and glycerol (Figure 4), thereby
585 highlighting its versatility. Further, OTU 1 also increased in no-substrate controls over time,
586 suggesting it either utilized natural organic matter in the microcosms, or fermentation products
587 produced from the degradation of the natural organic matter by other members of the community.
588
589 In addition to the relatively abundant taxa described above that were ^{13}C-enriched and
590 that could be linked to genomes or MAGs, we also identified ^{13}C-enrichment in several low
591 abundance taxa (<1% relative abundances), i.e., members of the genera *Photobacterium* (OTU
592 54), *Vibrio* (OTU 80) and *Fusibacter* (OTU 38). These taxa may have therefore played a lesser
593 role in the primary hydrolysis of the macromolecules and are therefore discussed briefly in the
594 Supplementary Discussion.
595

After the main primary degradation processes and increased formation of fermentation products (i.e., VFAs) in the first 5 days, ongoing depletion of sulfate and inhibition of sulfate depletion by molybdate indicated SRM were active. Various taxa including *Deltaproteobacteria* related to known SRM became ^{13}C-labelled at day 10, which suggested transfer of carbon from the added macromolecules to SRM. This was likely via oxidation of the VFAs by SRM, because deltaproteobacterial SRM are known to be important oxidizers of fermentation products in marine sediments [82–84]. The detection of more ^{13}C-labelled putative SRM of the *Deltaproteobacteria* from protein incubations than from lipid incubations may have reflected the more diverse taxa involved in primary degradation of the proteins, e.g., through more diverse metabolic interactions. We also hypothesize the additional nitrogen supply from the proteins may have facilitated the growth of more diverse *Deltaproteobacteria*, since none of the VFAs appeared to be limiting from either protein or lipid treatments.

In conclusion, this study provided new insights into the identities and functions of various protein- and lipid-degrading microorganisms in cold marine sediments and indicates *Psychromonas* spp. are prominent players in the utilization of fresh detrital protein and/or lipid macromolecules. The activity of these primary hydrolysers also facilitates relatively rapid transfer of carbon and energy among trophic levels within the sediment microbial community.

Acknowledgements

The authors would like to thank the crew of the R/V Sanna 2013 summer sampling campaign, which was funded by the Arctic Research Centre, Aarhus University, and Kasper Kjeldsen, Hans Røy and Marit-Solveig Seidenkranz for providing the sediment samples. We thank captain (Stig Henningsen) and first mate of MS Farm for their assistance during sampling of Svalbard sediments in 2017, as well as the Kings Bay Marine Laboratory and the AWIPEV Arctic Research Base in Ny-Ålesund for assistance and laboratory space. Furthermore the authors want to thank Carmen Czepe from the Vienna Biocenter Core Facilities Next Generation Sequencing facility for

sequencing of metagenomic libraries on the Illumina Hiseq2500 instrument. This work was financially supported by the Austrian Science Fund (P29426-B29 to KW; P25111-B22 to AL).

The authors declare no conflict of interest.

Figure legends

Figure 1. Concentration profiles of sulfate and fermentation products in subarctic marine sediment microcosms. Concentrations of sulfate (A) and volatile fatty acids (B) were determined in anoxic incubations with ^{13}C-protein or ^{13}C-lipids, and with or without the sulfate reduction inhibitor molybdate. Control microcosms were incubated without organic substrates and without molybdate.

Figure 2. 16S rRNA gene OTUs enriched in heavy ^{13}C-DNA-SIP gradient fractions. Heatmaps showing the relative abundance of 16S rRNA gene OTUs in DNA-SIP gradient fractions from anoxic sediment incubations amended with ^{13}C-proteins or ^{13}C-lipids and from unamended control incubations. Significant (FDR-adjusted p-value was <0.1) ^{13}C-enrichment was determined by differential abundance analysis between high density (^{13}C-enriched, >1.726 g ml^{-1}, pink blocks) and low density (^{13}C-free, <1.720 g ml^{-1}, turquoise blocks) DNA, and is indicated by filled circles. 16S rRNA genes that were matched to 16S rRNA gene sequences of genomes/MAGs are indicated in bold.

Figure 3. Differential ^{13}C-labeling and response of *Psychromonas* sub-OTUs in protein- and lipid-amended sediment microcosms. (A) Heatmap showing the relative abundance of four sub-OTUs of *Psychromonas* 16S rRNA OTU 4 in DNA-SIP gradients. Significant ^{13}C-enrichment was determined by differential abundance analysis between high density (^{13}C-enriched) and low density (^{12}C-enriched) DNA-SIP fractions. Sub-OTU 4, which was identical to the 16S rRNA gene

652 sequence of *Psychromonas* MAG GLG-1, is indicated in bold. (B) Phylogeny of *Psychromonas*
653 sub-OTUs. The sequences were aligned with MAFFT (Katoh et al., 2002) and the tree was
654 calculated with FastTree (Price et al., 2010). (C) Changes in relative abundance of *Psychromonas*
655 sub-OTUs in protein-amended, lipid-amended, and unamended sediment microcosms with or
656 without the sulfate reduction inhibitor molybdate.
657
658 **Figure 4. Genome-inferred metabolic models of protein- and lipid-degrading bacteria in**
659 **arctic marine sediment.** Schematic depiction of predicted metabolic properties of
660 *Psychrilyobacter atlanticus*, *Clostridia* MAG GPF-1, and *Psychromonas* MAG GLG-1, which
661 correspond to the 16S rRNA OTUs 5, 1, and 4, respectively. The models indicate macromolecule
662 degradation processes and enzymes that may explain the observed biogeochemical patterns and
663 the ^{13}C-enrichment of corresponding 16S rRNA OTUs in the DNA-SIP incubations. Enzymes that
664 are indicated in pale colour were not found in the respective genome/MAG. SS, Secretion system;
665 TCA, tricarboxylic acid cycle; TAT, Twin-arginine translocation pathway; SEC, Sec secretion
666 system; LIT, process has physiological evidence but the involved enzymes are not identified yet.
667
668

669 ## References

670 1. Hop H, Pearson T, Hegseth EN, Kovacs KM, Wiencke C, Kwasniewski S, et al. The marine
671 ecosystem of Kongsfjorden, Svalbard. *Polar Res* 2002; **21**: 167–208.
672 2. Arndt S, Jørgensen BB, LaRowe DE, Middelburg JJ, Pancost RD, Regnier P. Quantifying
673 the degradation of organic matter in marine sediments: A review and synthesis. *Earth-Sci*
674 *Rev* 2013; **123**: 53–86.
675 3. Dunne JP, Sarmiento JL, Gnanadesikan A. A synthesis of global particle export from the
676 surface ocean and cycling through the ocean interior and on the seafloor. *Global*
677 *Biogeochem Cycles* 2007; **21**: 1–16.
678 4. Christian JR, Karl DM. Bacterial ectoenzymes in marine waters: Activity ratios and
679 temperature responses in three oceanographic provinces. *Limnol Oceanogr* 1995; **40**:

1042–1049.

5. Fabiano M, Pusceddu A. Total and hydrolizable particulate organic matter (carbohydrates, proteins and lipids) at a coastal station in Terra Nova Bay (Ross Sea, Antarctica). *Polar Biol* 1998; **19**: 125–132.

6. Bradley JA, Amend JP, LaRowe DE. Necromass as a Limited Source of Energy for Microorganisms in Marine Sediments. *J Geophys Res Biogeosci* 2018; **123**: 577–590.

7. Wehrmann LM, Formolo MJ, Owens JD, Raiswell R, Ferdelman TG, Riedinger N, et al. Iron and manganese speciation and cycling in glacially influenced high-latitude fjord sediments (West Spitsbergen, Svalbard): Evidence for a benthic recycling-transport mechanism. *Geochim Cosmochim Acta* 2014; **141**: 628–655.

8. Burdige DJ. Preservation of organic matter in marine sediments: controls, mechanisms, and an imbalance in sediment organic carbon budgets? *Chem Rev* 2007; **107**: 467–485.

9. Hedges JI, Oades JM. Comparative organic geochemistries of soils and marine sediments. *Org Geochem* 1997; **27**: 319–361.

10. McCarthy M, Pratum T, Hedges J, Benner R. Chemical composition of dissolved organic nitrogen in the ocean. *Nature* 1997; **390**: 150–154.

11. Vetter YA, Deming JW. Extracellular enzyme activity in the Arctic Northeast Water polynya. *Mar Ecol Prog Ser* 1994; **114**: 23–34.

12. Parsons TR, Stephens K, Strickland JDH. On the Chemical Composition of Eleven Species of Marine Phytoplankters. *J Fish Res Board Can* 1961; **18**: 1001–1016.

13. Hudson BJ, Karis IG. The lipids of the alga Spirulina. *J Sci Food Agric* 1974; **25**: 759–763.

14. Wakeham SG, Lee C, Farrington JW, Gagosian RB. Biogeochemistry of particulate organic matter in the oceans: results from sediment trap experiments. *Deep Sea Res A* 1984; **31**: 509–528.

15. Harvey HR, Rodger Harvey H, Fallon RD, Patton JS. The effect of organic matter and oxygen on the degradation of bacterial membrane lipids in marine sediments. *Geochim Cosmochim Acta* 1986; **50**: 795–804.

16. Sousa DZ, Smidt H, Alves MM, Stams AJM. Ecophysiology of syntrophic communities that degrade saturated and unsaturated long-chain fatty acids. *FEMS Microbiol Ecol* 2009; **68**:

709 257–272.
710 17. Meyer-Reil L-A. Ecological Aspects of Enzymatic Activity in Marine Sediments.
711 *Brock/Springer Series in Contemporary Bioscience*. 1991. pp 84–95.
712 18. Beulig F, Røy H, Glombitza C, Jørgensen BB. Control on rate and pathway of anaerobic
713 organic carbon degradation in the seabed. *Proc Natl Acad Sci U S A* 2018; **115**: 367–372.
714 19. Arnosti C. Microbial extracellular enzymes and the marine carbon cycle. *Ann Rev Mar Sci*
715 2011; **3**: 401–425.
716 20. Arnosti C. Contrasting patterns of peptidase activities in seawater and sediments: An
717 example from Arctic fjords of Svalbard. *Mar Chem* 2015; **168**: 151–156.
718 21. Muyzer G, Stams AJM. The ecology and biotechnology of sulphate-reducing bacteria. *Nat*
719 *Rev Microbiol* 2008; **6**: 441–454.
720 22. Webster G, Watt LC, Rinna J, Fry JC, Evershed RP, Parkes RJ, et al. A comparison of
721 stable-isotope probing of DNA and phospholipid fatty acids to study prokaryotic functional
722 diversity in sulfate-reducing marine sediment enrichment slurries. *Environ Microbiol* 2006;
723 **8**: 1575–1589.
724 23. Müller AL, Pelikan C, de Rezende JR, Wasmund K, Putz M, Glombitza C, et al. Bacterial
725 interactions during sequential degradation of cyanobacterial necromass in a sulfidic arctic
726 marine sediment. *Environ Microbiol* 2018; **20**: 2927–2940.
727 24. Knoblauch C, Sahm K, Jørgensen BB. Psychrophilic sulfate-reducing bacteria isolated from
728 permanently cold arctic marine sediments: description of *Desulfofrigus oceanense* gen.
729 nov., sp. nov., *Desulfofrigus fragile* sp. nov., *Desulfofaba gelida* gen. nov., sp. nov.,
730 *Desulfotalea psychrophila* gen. nov., sp. nov. and *Desulfotalea arctica* sp. nov. *Int J Syst*
731 *Bacteriol* 1999; **49**: 1631–1643.
732 25. Sahm K, Knoblauch C, Amann R. Phylogenetic affiliation and quantification of psychrophilic
733 sulfate-reducing isolates in marine Arctic sediments. *Appl Environ Microbiol* 1999; **65**:
734 3976–3981.
735 26. Na H, Lever MA, Kjeldsen KU, Schulz F, Jørgensen BB. Uncultured Desulfobacteraceae
736 and Crenarchaeotal group C3 incorporate 13C-acetate in coastal marine sediment. *Environ*
737 *Microbiol Rep* 2015; **7**: 614–622.

738 27. Wasmund K, Mußmann M, Loy A. The life sulfuric: microbial ecology of sulfur cycling in
739 marine sediments. *Environ Microbiol Rep* 2017; **9**: 323–344.
740 28. Lloyd KG, Schreiber L, Petersen DG, Kjeldsen KU, Lever MA, Steen AD, et al. Predominant
741 archaea in marine sediments degrade detrital proteins. *Nature* 2013; **496**: 215–218.
742 29. Zinke LA, Glombitza C, Bird JT, Røy H, Jørgensen BB, Lloyd KG, et al. Microbial organic
743 matter degradation potential in Baltic Sea sediments influenced by depositional conditions
744 and in situ geochemistry. *Appl Environ Microbiol* 2018; **85**: e02164–18.
745 30. Orsi WD, Richards TA, Francis WR. Predicted microbial secretomes and their target
746 substrates in marine sediment. *Nat Microbiol* 2018; **3**: 32–37.
747 31. Baker BJ, Lazar CS, Teske AP, Dick GJ. Genomic resolution of linkages in carbon,
748 nitrogen, and sulfur cycling among widespread estuary sediment bacteria. *Microbiome*
749 2015; **3**: 14.
750 32. Boyer T, Levitus S, Garcia H, Locarnini RA, Stephens C, Antonov J. Objective analyses of
751 annual, seasonal, and monthly temperature and salinity for the World Ocean on a 0.25 grid.
752 *International Journal of Climatology: A Journal of the Royal Meteorological Society* 2005;
753 **25**: 931–945.
754 33. Graue J, Engelen B, Cypionka H. Degradation of cyanobacterial biomass in anoxic tidal-flat
755 sediments: a microcosm study of metabolic processes and community changes. *ISME J*
756 2012; **6**: 660–669.
757 34. Newport PJ, Nedwell DB. The mechanisms of inhibition of *Desulfovibrio* and
758 *Desulfotomaculum* species by selenate and molybdate. *J Appl Bacteriol* 1988; **65**: 419–
759 423.
760 35. Glombitza C, Pedersen J, Røy H, Jørgensen BB. Direct analysis of volatile fatty acids in
761 marine sediment porewater by two-dimensional ion chromatography-mass spectrometry.
762 *Limnol Oceanogr Methods* 2014; **12**: 455–468.
763 36. Dumont MG, Radajewski SM, Miguez CB, McDonald IR, Murrell JC. Identification of a
764 complete methane monooxygenase operon from soil by combining stable isotope probing
765 and metagenomic analysis. *Environ Microbiol* 2006; **8**: 1240–1250.
766 37. Neufeld JD, Vohra J, Dumont MG, Lueders T, Manefield M, Friedrich MW, et al. DNA

767 stable-isotope probing. *Nat Protoc* 2007; **2**: 860–866.
768 38. Pelikan C, Herbold CW, Hausmann B, Müller AL, Pester M, Loy A. Diversity analysis of
769 sulfite- and sulfate-reducing microorganisms by multiplex *dsrA* and *dsrB* amplicon
770 sequencing using new primers and mock community-optimized bioinformatics. *Environ*
771 *Microbiol* 2016; **18**: 2994–3009.
772 39. Herbold CW, Pelikan C, Kuzyk O, Hausmann B, Angel R, Berry D, et al. Corrigendum: A
773 flexible and economical barcoding approach for highly multiplexed amplicon sequencing of
774 diverse target genes. *Front Microbiol* 2016; **7**: 870.
775 40. Tikhonov M, Leach RW, Wingreen NS. Interpreting 16S metagenomic data without
776 clustering to achieve sub-OTU resolution. *ISME J* 2015; **9**: 68–80.
777 41. Love MI, Huber W, Anders S. Moderated estimation of fold change and dispersion for RNA-
778 seq data with DESeq2. *Genome Biol* 2014; **15**: 550.
779 42. Orsi WD, Smith JM, Liu S, Liu Z, Sakamoto CM, Wilken S, et al. Diverse, uncultivated
780 bacteria and archaea underlying the cycling of dissolved protein in the ocean. *ISME J* 2016;
781 **10**: 2158–2173.
782 43. Lagkouvardos I, Joseph D, Kapfhammer M, Giritli S, Horn M, Haller D, et al. IMNGS: A
783 comprehensive open resource of processed 16S rRNA microbial profiles for ecology and
784 diversity studies. *Sci Rep* 2016; **6**: 33721.
785 44. Peng Y, Leung HCM, Yiu SM, Chin FYL. IDBA-UD: a de novo assembler for single-cell and
786 metagenomic sequencing data with highly uneven depth. *Bioinformatics* 2012; **28**: 1420–
787 1428.
788 45. Bankevich A, Nurk S, Antipov D, Gurevich AA, Dvorkin M, Kulikov AS, et al. SPAdes: a new
789 genome assembly algorithm and its applications to single-cell sequencing. *J Comput Biol*
790 2012; **19**: 455–477.
791 46. Li H, Durbin R. Fast and accurate short read alignment with Burrows-Wheeler transform.
792 *Bioinformatics* 2009; **25**: 1754–1760.
793 47. Li H, Handsaker B, Wysoker A, Fennell T, Ruan J, Homer N, et al. The Sequence
794 Alignment/Map format and SAMtools. *Bioinformatics* 2009; **25**: 2078–2079.
795 48. Kang DD, Froula J, Egan R, Wang Z. MetaBAT, an efficient tool for accurately

796 reconstructing single genomes from complex microbial communities. *PeerJ* 2015; **3**: e1165.
797 49. Wu Y-W, Simmons BA, Singer SW. MaxBin 2.0: an automated binning algorithm to recover
798 genomes from multiple metagenomic datasets. *Bioinformatics* 2016; **32**: 605–607.
799 50. Alneberg J, Bjarnason BS, de Bruijn I, Schirmer M, Quick J, Ijaz UZ, et al. Binning
800 metagenomic contigs by coverage and composition. *Nat Methods* 2014; **11**: 1144–1146.
801 51. Sieber CMK, Probst AJ, Sharrar A, Thomas BC, Hess M, Tringe SG, et al. Recovery of
802 genomes from metagenomes via a dereplication, aggregation and scoring strategy. *Nat*
803 *Microbiol* 2018; **3**: 836–843.
804 52. Olm MR, Brown CT, Brooks B, Banfield JF. dRep: a tool for fast and accurate genomic
805 comparisons that enables improved genome recovery from metagenomes through de-
806 replication. *ISME J* 2017; **11**: 2864–2868.
807 53. Parks DH, Imelfort M, Skennerton CT, Hugenholtz P, Tyson GW. CheckM: assessing the
808 quality of microbial genomes recovered from isolates, single cells, and metagenomes.
809 *Genome Res* 2015; **25**: 1043–1055.
810 54. Parks DH, Chuvochina M, Waite DW, Rinke C, Skarshewski A, Chaumeil P-A, et al. A
811 standardized bacterial taxonomy based on genome phylogeny substantially revises the tree
812 of life. *Nat Biotechnol* 2018; **36**: 996–1004.
813 55. Chaumeil P-A, Mussig AJ, Hugenholtz P, Parks DH. GTDB-Tk: a toolkit to classify
814 genomes with the Genome Taxonomy Database. *Bioinformatics* 2019.
815 56. Nguyen L-T, Schmidt HA, von Haeseler A, Minh BQ. IQ-TREE: a fast and effective
816 stochastic algorithm for estimating maximum-likelihood phylogenies. *Mol Biol Evol* 2015;
817 **32**: 268–274.
818 57. Minh BQ, Nguyen MAT, von Haeseler A. Ultrafast approximation for phylogenetic
819 bootstrap. *Mol Biol Evol* 2013; **30**: 1188–1195.
820 58. Letunic I, Bork P. Interactive Tree Of Life (iTOL): an online tool for phylogenetic tree display
821 and annotation. *Bioinformatics* 2007; **23**: 127–128.
822 59. Jain C, Rodriguez-R LM, Phillippy AM, Konstantinidis KT, Aluru S. High throughput ANI
823 analysis of 90K prokaryotic genomes reveals clear species boundaries. *Nat Commun* 2018;
824 **9**: 5114.

825 60. Vallenet D, Calteau A, Cruveiller S, Gachet M, Lajus A, Josso A, et al. MicroScope in 2017:
826 an expanding and evolving integrated resource for community expertise of microbial
827 genomes. *Nucleic Acids Res* 2017; **45**: D517–D528.
828 61. Aziz RK, Bartels D, Best AA, DeJongh M, Disz T, Edwards RA, et al. The RAST Server:
829 rapid annotations using subsystems technology. *BMC Genomics* 2008; **9**: 75.
830 62. Buchfink B, Xie C, Huson DH. Fast and sensitive protein alignment using DIAMOND. *Nat*
831 *Methods* 2015; **12**: 59–60.
832 63. Jones P, Binns D, Chang H-Y, Fraser M, Li W, McAnulla C, et al. InterProScan 5: genome-
833 scale protein function classification. *Bioinformatics* 2014; **30**: 1236–1240.
834 64. Finn RD, Bateman A, Clements J, Coggill P, Eberhardt RY, Eddy SR, et al. Pfam: the
835 protein families database. *Nucleic Acids Res* 2013; **42**: D222–D230.
836 65. Haft DH, Selengut JD, White O. The TIGRFAMs database of protein families. *Nucleic Acids*
837 *Res* 2003; **31**: 371–373.
838 66. UniProt Consortium T. UniProt: the universal protein knowledgebase. *Nucleic Acids Res*
839 2018; **46**: 2699.
840 67. Kall L, Krogh A, Sonnhammer ELL. Advantages of combined transmembrane topology and
841 signal peptide prediction--the Phobius web server. *Nucleic Acids Res* 2007; **35**: W429–
842 W432.
843 68. Yu NY, Wagner JR, Laird MR, Melli G, Rey S, Lo R, et al. PSORTb 3.0: improved protein
844 subcellular localization prediction with refined localization subcategories and predictive
845 capabilities for all prokaryotes. *Bioinformatics* 2010; **26**: 1608–1615.
846 69. Rawlings ND. MEROPS: the peptidase database. *Nucleic Acids Res* 2000; **28**: 323–325.
847 70. Lenfant N, Hotelier T, Velluet E, Bourne Y, Marchot P, Chatonnet A. ESTHER, the
848 database of the α/β-hydrolase fold superfamily of proteins: tools to explore diversity of
849 functions. *Nucleic Acids Res* 2013; **41**: D423–9.
850 71. Lombard V, Ramulu HG, Drula E, Coutinho PM, Henrissat B. The carbohydrate-active
851 enzymes database (CAZy) in 2013. *Nucleic Acids Res* 2014; **42**: D490–D495
852 72. Altschul SF, Madden TL, Schäffer AA, Zhang J, Zhang Z, Miller W, et al. Gapped BLAST
853 and PSI-BLAST: a new generation of protein database search programs. *Nucleic Acids Res*

854 1997; **25**: 3389–3402.
855 73. Steen AD, Kevorkian RT, Bird JT, Dombrowski N, Baker BJ, Hagen SM, et al. Kinetics and
856 Identities of Extracellular Peptidases in Subsurface Sediments of the White Oak River
857 Estuary, North Carolina. *Appl Environ Microbiol* 2019; **85**.
858 74. Pruesse E, Peplies J, Glöckner FO. SINA: accurate high-throughput multiple sequence
859 alignment of ribosomal RNA genes. *Bioinformatics* 2012; **28**: 1823–1829.
860 75. Quast C, Pruesse E, Yilmaz P, Gerken J, Schweer T, Yarza P, et al. The SILVA ribosomal
861 RNA gene database project: improved data processing and web-based tools. *Nucleic Acids*
862 *Res* 2013; **41**: D590–6.
863 76. Price MN, Dehal PS, Arkin AP. FastTree 2 – Approximately Maximum-Likelihood Trees for
864 Large Alignments. *PLoS One* 2010; **5**: e9490.
865 77. Berger SA, Krompass D, Stamatakis A. Performance, accuracy, and Web server for
866 evolutionary placement of short sequence reads under maximum likelihood. *Syst Biol* 2011;
867 **60**: 291–302.
868 78. Stamatakis A. RAxML version 8: a tool for phylogenetic analysis and post-analysis of large
869 phylogenies. *Bioinformatics* 2014; **30**: 1312–1313.
870 79. Zhao J-S, -S. Zhao J, Manno D, Hawari J. Psychrilyobacter atlanticus gen. nov., sp. nov., a
871 marine member of the phylum Fusobacteria that produces H2 and degrades nitramine
872 explosives under low temperature conditions. *Int J Syst Evol Microbiol* 2009; **59**: 491–497.
873 80. Wakeham SG, Canuel EA. Degradation and Preservation of Organic Matter in Marine
874 Sediments. *The Handbook of Environmental Chemistry*. 2006. pp 295–321.
875 81. Bienhold C, Boetius A, Ramette A. The energy–diversity relationship of complex bacterial
876 communities in Arctic deep-sea sediments. *ISME J* 2011; **6**: 724–732.
877 82. Glombitza C, Jaussi M, Røy H, Seidenkrantz M-S, Lomstein BA, Jørgensen BB. Formate,
878 acetate, and propionate as substrates for sulfate reduction in sub-arctic sediments of
879 Southwest Greenland. *Front Microbiol* 2015; **6**: 846.
880 83. Finke N, Vandieken V, Jørgensen BB. Acetate, lactate, propionate, and isobutyrate as
881 electron donors for iron and sulfate reduction in Arctic marine sediments, Svalbard. *FEMS*
882 *Microbiology Ecology* . 2007. , **59**: 10–22

84. Glombitza C, Egger M, Røy H, Jørgensen BB. Controls on volatile fatty acid concentrations in marine sediments (Baltic Sea). *Geochim Cosmochim Acta* 2019; **258**: 226–241.

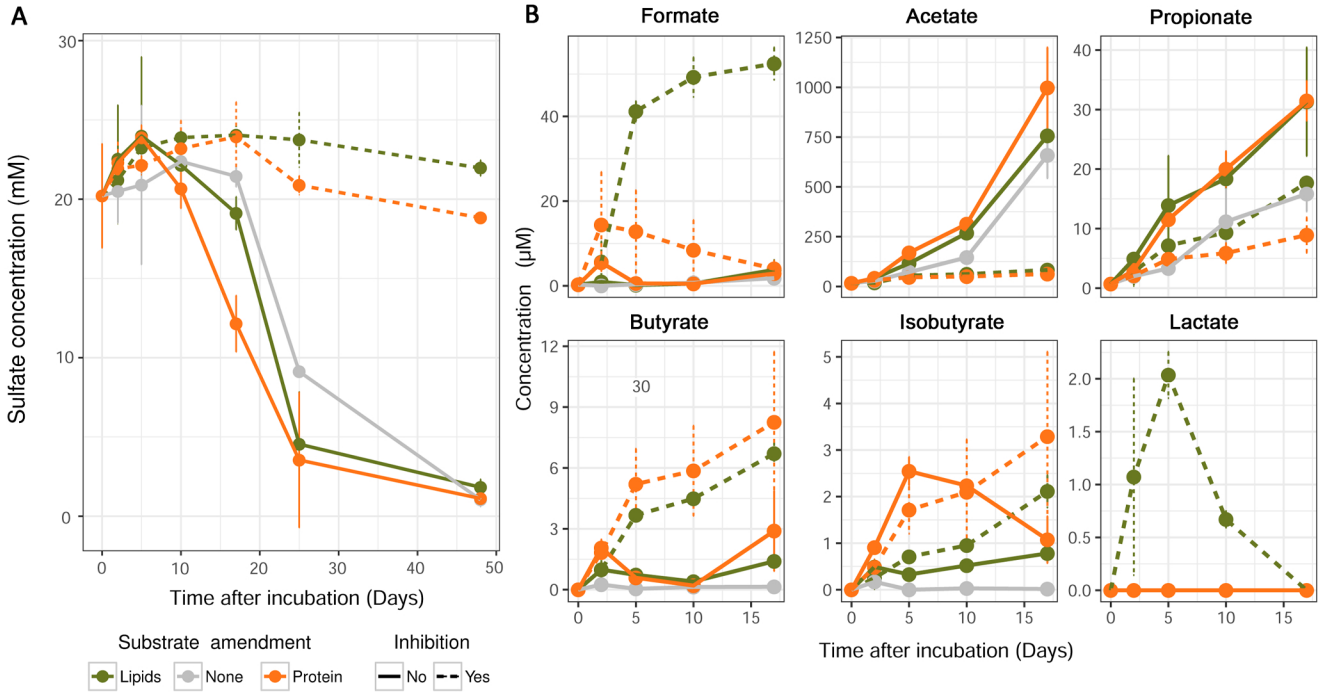

Figure 1. Concentration profiles of sulfate and fermentation products in subarctic marine sediment microcosms. Concentrations of sulfate (A) and volatile fatty acids (B) were determined in anoxic incubations with ^{13}C-protein or ^{13}C-lipids, and with or without the sulfate reduction inhibitor molybdate. Control microcosms were incubated without organic substrates and without molybdate. Error bars indicate standard deviation.

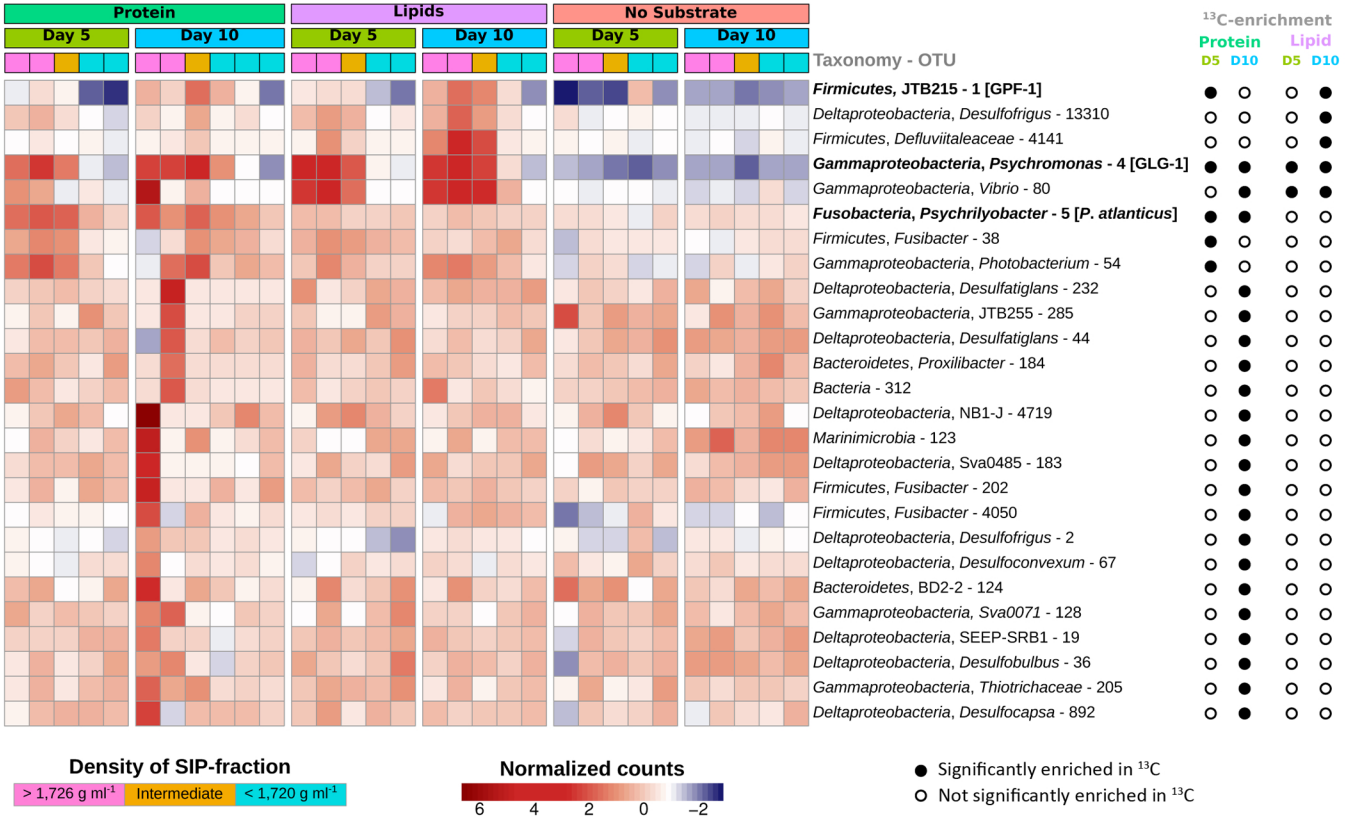

Figure 2. 16S rRNA gene OTUs enriched in heavy ^{13}C-DNA-SIP gradient fractions. Heatmaps showing the relative abundance of 16S rRNA gene OTUs in DNA-SIP gradient fractions from anoxic sediment incubations amended with ^{13}C-proteins or ^{13}C-lipids and from unamended control incubations. Significant (FDR-adjusted p-value was below 0.1) ^{13}C-enrichment was determined by differential abundance analysis between high density (^{13}C-enriched, >1.726 g ml^{-1}, pink blocks) and low density (^{13}C-free, <1.720 g ml^{-1}, turquoise blocks) DNA, and is indicated by filled circles. 16S rRNA genes that were matched to 16S rRNA gene sequences of genomes/MAGs are indicated in bold.

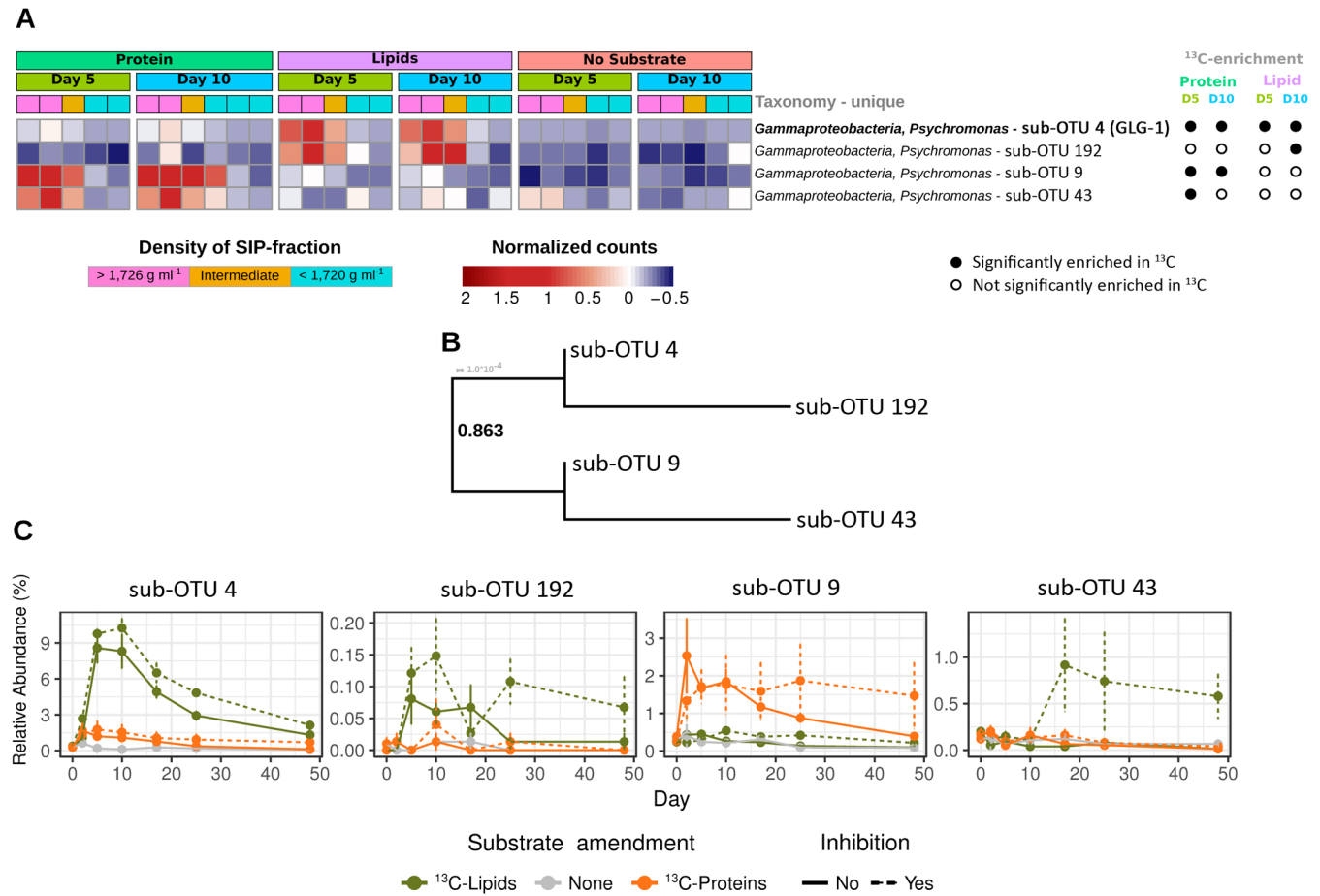

Figure 3. Differential ^{13}C-labeling and response of *Psychromonas* sub-OTUs in protein- and lipid-amended sediment microcosms. (A) Heatmap showing the relative abundance of four sub-OTUs of *Psychromonas* 16S rRNA OTU 4 in DNA-SIP gradients. Significant ^{13}C-enrichment was determined by differential abundance analysis between high density (^{13}C-enriched) and low density (^{12}C-enriched) DNA-SIP fractions. sOTU 4, which was identical to the 16S rRNA gene sequence of *Psychromonas* MAG GLG-1, is indicated in bold. (B) Phylogeny of *Psychromonas* sub-OTUs. The sequences were aligned with MAFFT (Katoh et al., 2002) and the tree was calculated with FastTree (Price et al., 2010). (C) Changes in relative abundance of *Psychromonas* sub-OTUs in protein-amended, lipid-amended, and unamended sediment microcosms with or without the sulfate reduction inhibitor molybdate.

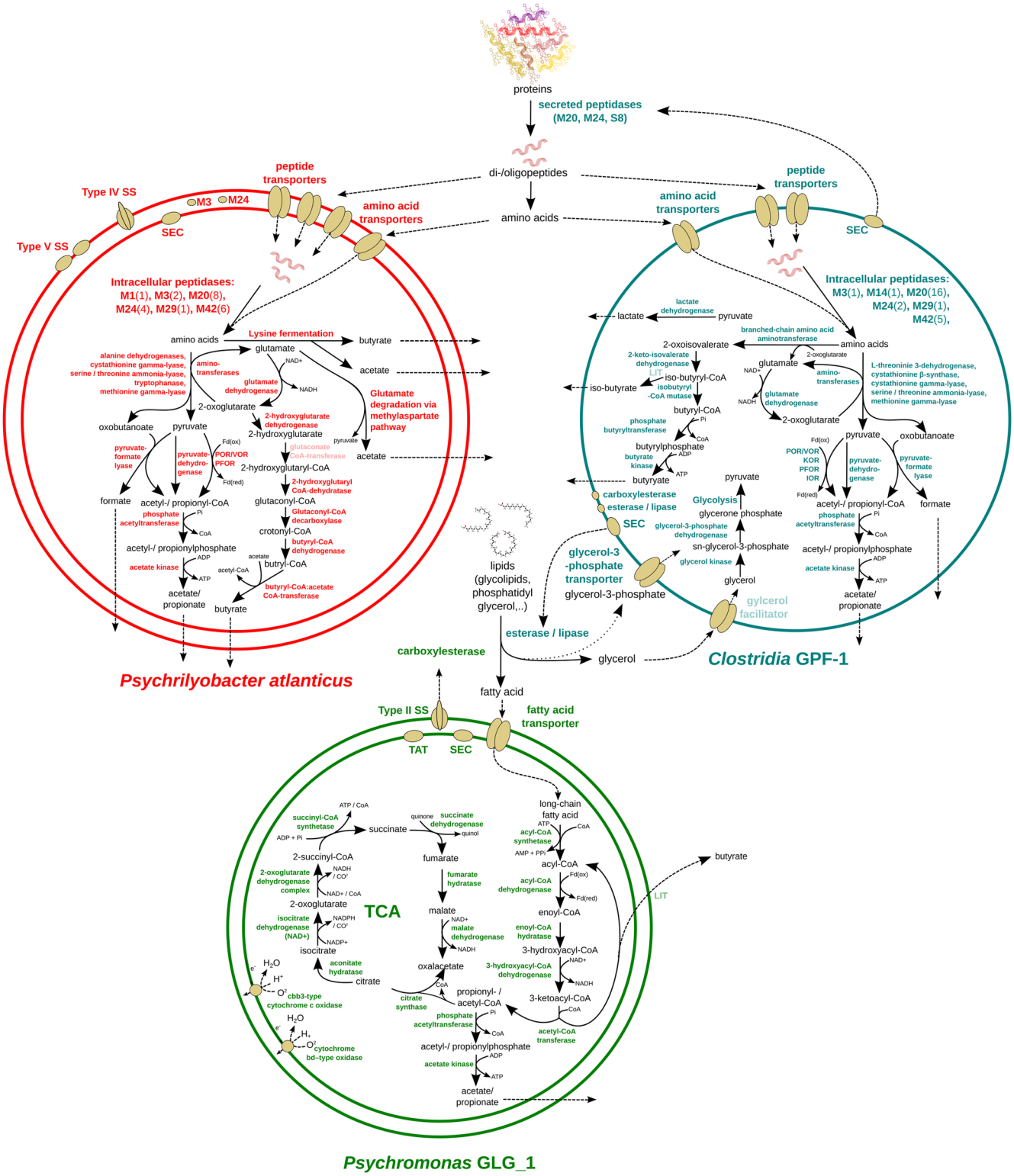

Figure 4. Genome-inferred metabolic models of protein- and lipid-degrading bacteria in arctic marine sediment. Schematic depiction of predicted metabolic properties of *Psychrilyobacter atlanticus*, *Clostridia* MAG GPF-1, and *Psychromonas* MAG GLG-1, which correspond to the 16S rRNA OTUs 5, 1, and 4, respectively. The models indicate macromolecule degradation processes and enzymes that may explain the observed biochemical patterns and the ^{13}C-enrichment of corresponding 16S rRNA OTUs in the DNA-SIP incubations. Enzymes that are indicated in pale colour were not found in the respective genome/MAG. SS, Secretion system; TCA, tricarboxylic acid cycle; TAT, Twin-arginine translocation pathway; SEC, Sec secretion system; LIT, process has physiological evidence but the involved enzymes are not identified yet.